Proceedings of 20th International Congress on Acoustics, ICA 2010

23-27 August 2010, Sydney, Australia

Acoustic sensitivity to micro-perturbations of KEMAR's pinna surface geometry

Parham Mokhtari, Hironori Takemoto, Ryouichi Nishimura and Hiroaki Kato

National Institute of Information and Communications Technology (NICT),
2-2-2 Hikaridai, Seikacho, "Keihanna Science City", Kyoto 619-0288, Japan

PACS: 43.64.Ha, 43.20.Ks, 43.20.El, 43.20.Fn

ABSTRACT

To better understand the relations between pinna anthropometry and acoustic features used for sound localisation, acoustic sensitivity analysis was carried out on the DB60 pinna of the Knowles Electronics Manikin for Acoustic Research (KEMAR), with the aid of computer simulations with the Finite-Difference Time Domain (FDTD) method. Starting with the original shape of the pinna and an adjacent patch of KEMAR's head voxelated on a uniform 3D grid of resolution 2 mm, FDTD simulation was used to obtain a baseline set of Pinna-Related Transfer Functions (PRTFs) at 45 spatial locations covering a wide range of azimuth and elevation angles, a distance 1 m from the ear. A total of 1784 unique "micro"-perturbations were then effected by adding a single voxel at a time along the entire outer surface of the pinna and adjoining head-side. For each perturbation, a full set of PRTFs were obtained by simulation and compared with the original PRTFs, to precisely quantify the resulting shifts in the centre-frequencies of 234 acoustic features (at most 4 peaks and 3 notches per PRTF, across 45 spatial locations) that appeared up to 14 kHz. This large amount of data allowed the creation of detailed 3D maps of the pinna showing patterns of frequency sensitivity for every peak and notch, thus revealing the anatomical parts of the pinna most strongly affiliated with each acoustic feature. A measure of correlation was used to group the 234 pinna sensitivity maps into a smaller number of distinct categories. The results contribute to knowledge on the physical modes of pinna resonance and anti-resonance.

INTRODUCTION

It is well known that human performance in sound localisation is compromised if one's own head-related transfer functions (HRTFs) are not available. HRTF personalisation is therefore necessary in spatial audio and related applications, to account for the unique geometry of each person's head and external ears (pinnae). However, a major impediment to effective personalisation of HRTFs, is our incomplete knowledge on the causal relations between head and pinna geometry and HRTF acoustic features.

While structural models have been proposed to account for HRTF or head-related impulse response (HRIR) features caused by the head, torso and shoulders (e.g., Brown & Duda, 1998; Algazi *et al*., 2002), the connections between acoustic features and pinna anthropometry in particular are less well developed. And yet, numerous acoustic measurements and psychophysical experiments on sound localisation have confirmed the importance of monaural spectral cues provided by HRTF peaks and notches (e.g., Blauert, 1974; Iida, 2007), many of which are generated by the complex geometry of the pinna and are therefore evident in pinna-related transfer functions (PRTFs). As summarised below, the most important contributions to understanding the physical modes of pinna resonance that give rise to HRTF or PRTF peaks and notches, come from either acoustic measurements or computational models.

In pioneering work, Shaw & Teranishi (1968) measured acoustic pressure responses on a rubber replica of a baffled pinna. They were perhaps the first to reveal the physical manifestation of resonance modes, in schematic diagrams of the pinna showing the basic patterns of sound pressure in the concha and cymba cavities at particular frequencies corresponding to peaks in the transfer function. Subsequent measurements averaged over 10 real human ears with blocked meatus revealed that the broad spectral peak at 4.3 kHz was generated by a quarter-wavelength depth resonance of the entire concha, two peaks at 7.1 and 9.6 kHz were caused by vertical modes of resonance involving the concha, cymba and triangular fossa, and two higher peaks at 12.1 and 14.4 kHz were caused by horizontal transverse modes of resonance involving the front and back parts of the concha and cymba (Shaw, 1997).

In pioneering work on numerical simulation of acoustic pressure responses with the Boundary Element Method (BEM), Kahana & Nelson (2000; 2006) essentially replicated Shaw's (1997) pressure distribution patterns (notwithstanding differences in resonance frequencies and pattern details due to differences in pinna size and geometry). Thanks to the advantages of computer simulation over physical measurements, they were able to show pressure distribution patterns at high spatial resolution across the entire surface of the pinna. For the DB60 pinna of the Knowles Electronics Manikin for Acoustic Research (KEMAR), Kahana & Nelson (2000, Fig. 13) revealed a concha depth resonance at 4.5 kHz, two vertical resonances at 7.8 and 10.3 kHz, and two horizontal transverse resonances at 14.0 and 17.0 kHz. For KEMAR's slightly larger DB65 pinna, Kahana & Nelson (2006, Fig. 7) found a concha depth resonance at 4.2 kHz, two vertical

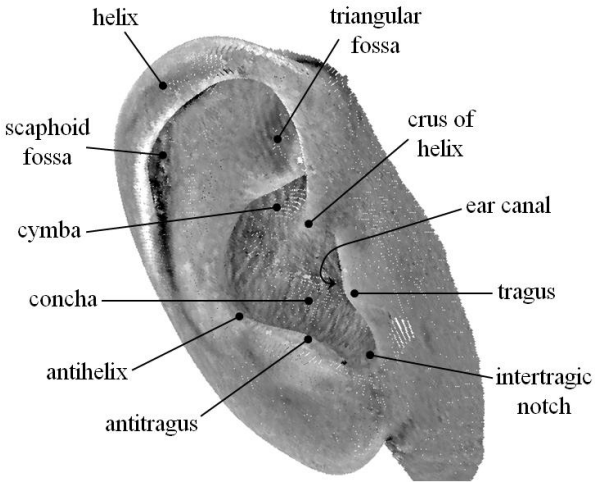

Figure 1. The DB60 right pinna, annotated with labels for the main anatomical features. The laser-scanned 3D surface data were kindly provided by Dr. Yuvi Kahana.

resonances at 7.2 and 9.5 kHz, and three horizontal transverse resonances at 11.6, 14.8 and 18.0 kHz. They then obtained similar results with other pinnae, using a more sophisticated method based on singular value decomposition (SVD) of the simulated acoustic pressure responses in order to identify orthogonal spatial modes of resonance.

While acoustic measurement and simulation methods have thus been used to characterise the pinna resonances that are associated with PRTF peaks, physical characterisation of HRTF or PRTF notches has been more elusive. The earliest explanations of notches were in terms of delay-and-add models that assumed cancellation of incoming acoustic waves near the ear-canal entrance with delayed reflections from the posterior wall of the concha (e.g., Hebrank & Wright, 1974; Raykar *et al*., 2005). However, more detailed physical modelling by Lopez-Poveda & Meddis (1996) concluded that both reflection and diffraction phenomena are required to more accurately predict the notch frequencies and their directional variations; in other words, they concluded that simple ray-based models of acoustic reflection are insufficient, and that diffraction and scattering of wavefronts across the entire surface of the concha (or indeed the entire pinna surface) must be taken into account.

More recently, with the Finite-Difference Time Domain (FDTD) method of acoustic simulation, Takemoto *et al*. (2009) were able to visualise not only the static modes of resonance revealed thus far, but also the dynamic evolution of acoustic wavefronts as they diffracted around and reflected from the pinna surface. Instantaneous pressure distribution patterns on pinnae of two male and two female subjects essentially confirmed the existence of a concha depth resonance and two vertical resonances similar to those measured by Shaw (1997). Additionally, dynamic visualisation allowed Takemoto *et al*. (2009) to clarify two different mechanisms of wave cancellation responsible for generating the first PRTF notch, which is known to be a strong spectral cue for elevation in the median plane (Iida *et al*., 2007).

In the present study we propose an alternative method of investigating the physical modes of pinna resonance, based on FDTD simulation and acoustic sensitivity analysis. Whereas all previous studies induced characteristic pressure distributions by driving the source at a selected peak or notch frequency at a time, our proposed method retains a broadband source typical in time-domain simulations. In this way, we propose to explicitly measure the shifts in the centre-frequencies of all observable peaks and notches, in response to micro-perturbations along the entire pinna surface. As described in the following sections that outline the methods and present the results, we were thus able to obtain detailed maps of pinna sensitivity for all peaks and notches within the simulated frequency bandwidth (up to 14 kHz) across a range of spatial locations all around the pinna.

METHODS

Pinna geometry data

In this study we used the DB60 right pinna of KEMAR (Burkhard & Sachs, 1975). The geometry data were kindly provided by Dr. Yuvi Kahana who had laser-scanned and later refined 3D coordinates of points on the surface of the entire right-half of the manikin's head, and at finer resolution the pinna alone. We used a semi-automatic procedure to optimally align the high-resolution pinna on the right-half head, and the combined data were reflected about the median plane to obtain a left-right symmetric whole head with pinnae. A close-up of the right pinna is shown in Fig. 1, together with labels for the main anatomical features.

The surface data were volumetrised on a 3D grid of uniform resolution 2 mm. This was done by comparing the centre of each grid voxel with the position and normal vector of the nearest surface point. The physical properties of each voxel (i.e., sound speed and material density) were then set to either air (outside the manikin) or water (inside the manikin). The open ear canals were closed by replacing air voxels with water, thus achieving blocked meatus conditions.

While we had previously used the volumetric whole-head data to verify our simulation methods (Mokhtari *et al*., 2009), in the present study we sought to alleviate the computational burden imposed by the hundreds of simulations required by sensitivity analysis. We therefore extracted a volume enclosing only the right pinna and an adjacent 6.2 x 8.4 cm patch of KEMAR's head. This head-patch provided a naturally-shaped baffle; to compensate for its necessarily finite size, the back and sides were terminated by absorbing boundary layers at the sides of the computation domain, as described below.

Acoustic simulation methods

FDTD simulation on the volumetric data was run with the computation domain bounded by an optimum Perfectly Matched Layer (oPML) of width 10 cells (Mokhtari *et al*., 2010). The patch of KEMAR's head was extended partially into the oPML at five adjacent sides of the computation domain, in order to avoid artefactual reflections and wave propagation behind or around the sides of the patch. FDTD temporal and spatial derivatives were accurate to 2nd and 4th order, respectively. Computation load was reduced by employing the acoustic reciprocity principle, wherein a point source was placed at the pinna and the developed pressure was observed at all spatial locations of interest in a single run. Computation and memory load were further reduced significantly by including the Kirchhoff-Helmholtz integral equation within the FDTD algorithm (Mokhtari *et al*., 2008), thereby allowing computation of acoustic pressure at any distance from the pinna, from the pressures developed on a closely surrounding integration surface.

In this way, far-field pressure responses were obtained at 45 spatial locations, a distance 1 m from the head centre (see Fig. 2). At a simulation sampling rate of about 1.3 MHz (determined by FDTD stability considerations for a 2 mm grid and for a maximum speed of sound in water; cf. Taflove & Brodwin, 1975), the far-field pressure responses over a duration of 5 ms were calculated starting from about 2.6 ms after

the onset of source excitation at the pinna, i.e., after the time taken for the wavefront to travel from the surrounding integration surface to the nearest far-field observation point.

The PRTF at each location was then calculated by normalising the Fourier magnitude spectrum of the pressure response, with that obtained under free-field conditions (i.e., with the same simulation but with all voxels set to air). No smoothing or windowing was applied, but in order to attain a sufficiently high frequency resolution all PRTFs (in dB) were resampled by cubic-spline interpolation, at 1 Hz resolution on a linear frequency scale from 500 Hz to 14 kHz. This upper limit of 14 kHz was determined by the simulation source characteristics, which in turn were set according to FDTD stability and accuracy criteria assuming that the shortest wavelength (i.e., the highest frequency) should be represented by at least 12 grid cells (voxels).

From a computational perspective, it is interesting to note that when our FDTD program (C code) was run on a 3 GHz processor, simulation of the far-field pressure waveforms used to calculate HRTFs for the whole-head data took about 2.5 hrs, while simulation with the smaller, baffled pinna yielding PRTFs took only about 5 min. This represented a 30-fold reduction in run-time, which offered significant savings in our sensitivity analysis requiring hundreds of simulations.

Acoustic feature extraction & sensitivity analysis

Having thus obtained a complete set of PRTFs under baseline conditions (see the black curves in Fig. 3), a peak-picking algorithm was used to extract the centre-frequencies and amplitudes of all observable peaks and notches. Up to 14 kHz there were at most 4 peaks and 3 notches per PRTF, and a total of 234 features across all 45 locations. These data served as reference acoustic features for the original pinna geometry, with which all perturbation results would be compared.

To define the micro-perturbations, a total of 1784 unique voxels of air were identified as lying directly adjacent to the surface of the pinna and head-patch. A total of 1784 additional simulations were therefore run, after converting each of these voxels at a time, from air to water; in effect, each perturbation placed a small, 2 mm bump on the original voxelated surface, thereby either reducing the volume of a cavity or extending an anatomical protuberance.

The PRTFs simulated after each micro-perturbation were compared with the baseline PRTFs, and a peak-picking algorithm guided by the reference set of centre-frequencies was used to quantify the frequency shifts in all the peaks and notches, to 1 Hz accuracy. Consistent with Ehrenfest's theorem which states that for small adiabatic perturbations of an undamped linear oscillator the *relative frequency shift* is equal to the *relative change in energy* of the oscillator (e.g., Schroeder, 1967), every frequency shift (dF) was normalised with respect to its original centre-frequency, thus transforming the data to a relative scale (dF/F).

Pinna pattern grouping & acoustic feature labelling

It is trivial to label the features of any single PRTF by progressive numbering from low to high frequencies (e.g., P1, P2, ..., for the peaks, and N1, N2, ..., for the notches). However, due to variations in peak or notch centre-frequency with spatial location and the absence or reappearance of certain features at some locations, it is considerably more difficult to assign labels that are also *spatially consistent* across all locations. As seen in Fig. 3, this was especially true of the second peak (P2) which appeared in PRTFs at only 7 locations; and

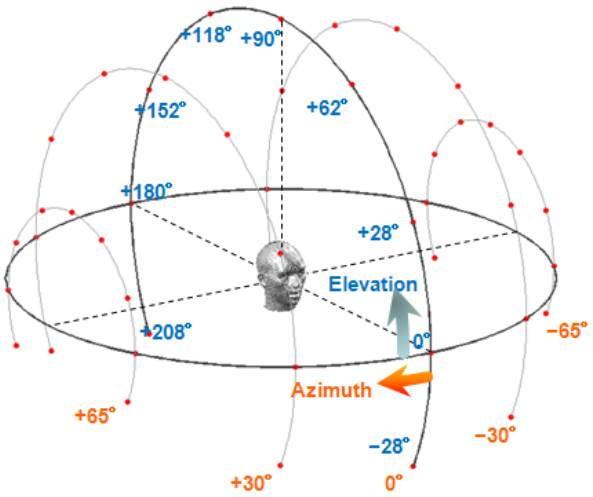

Figure 2. Spatial locations of 45 observation points a uniform distance 1 m from KEMAR's head centre, at all combinations of 5 azimuth and 9 elevation angles specified in *inter-aural polar* coordinates. While the whole head is included in this figure (drawn to scale), the FDTD simulations in the present study included only the right pinna and an adjacent patch of the head.

the first two notches (N1 and N2), whose centre-frequencies (and even presence or absence) varied substantially across locations, generally following a rise-fall trajectory across elevation angles (as amply documented in the literature).

Fortunately, the results of the sensitivity analysis suggested a way to overcome this problem. While a nominal label was initially assigned to each of the reference peaks and notches in order to aid in the calculation and analysis of frequency shifts (cf. Fig. 3), a more consistent and meaningful labelling was carried out *a posteriori* by grouping together those acoustic features whose pinna sensitivity patterns were sufficiently similar. In particular, treating each pattern as a vector of relative frequency-shift values, the coefficient of linear correlation between pairs of vectors was used as a measure of similarity between the corresponding pair of patterns. The 234 original patterns were thus classified into a smaller number of distinct groups, with the constraint that all patterns within a group should have a correlation no less than a minimum threshold (e.g., 0.8) with respect to the group mean. Consequently, the peaks or notches associated with the patterns in each group could be considered as having essentially similar physical resonance properties and, by extension, similar physical generative mechanisms.

RESULTS AND DISCUSSIONS

Baseline PRTFs & comparison with HRTFs

The black curves in Fig. 3 show the set of 45 simulated PRTFs, together with our tentative labelling of all 234 peaks and notches. The red dashed curves underlayed for comparison are the right-ear HRTFs simulated with the KEMAR whole head, which we had verified with independent acoustic measurements, reporting a mean spectral distortion of only 2.3 dB (Mokhtari *et al*., 2009). Comparison of these two sets of transfer functions revealed the acoustic effects of the head. As expected from previous simulations involving variously morphed head shapes (Mokhtari *et al*., 2009), differences were largest in the head shadow region on the far contralateral side (here at azimuth −65°), especially due to the appearance of a number of head-diffraction notches. Notwithstanding these and other smaller differences, on the whole Fig. 3

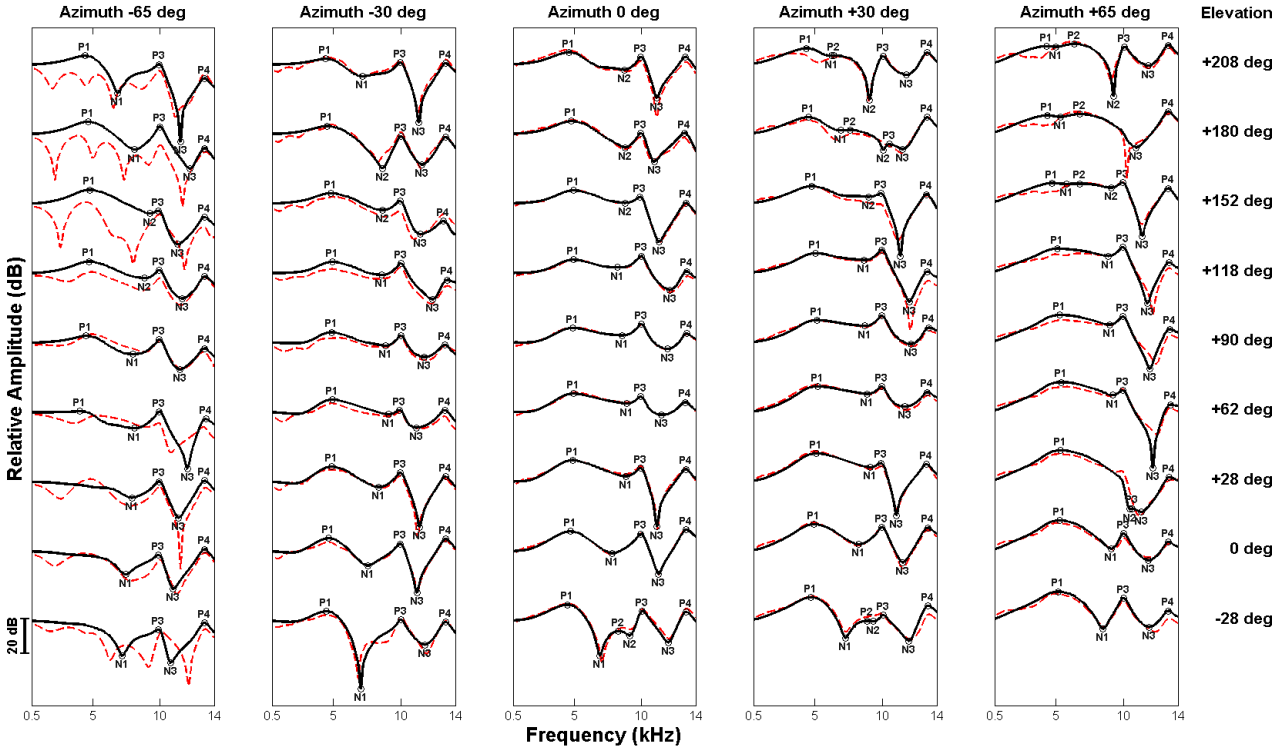

Figure 3. Comparison of baseline simulated PRTFs (solid black curves) at the 45 spatial locations shown in Fig. 2, with the simulated whole-head HRTFs (dashed red curves) obtained by Mokhtari *et al*. (2009) at the same locations. Also shown are the 234 PRTF reference peaks and notches, nominally labelled.

confirms for a wide range of locations what Takemoto *et al*. (2009) showed for the median plane: that the basic resonance and anti-resonance characteristics of HRTFs are also manifest in PRTFs, and that the majority of prominent HRTF peaks and notches are therefore caused mainly by the pinna.

In Fig. 3 it can be seen that of all the labelled acoustic features, the three peaks P1, P3 and P4 were the most consistent, appearing clearly at most locations and with a fairly small range of frequency variations around their respective mean values of 4.8, 10.0 and 13.3 kHz. In contrast, P2 appeared at only 7 locations, with a mean value of 7.3 kHz; it appeared most clearly at low front in the median plane, and more subtly as a broad spectral hump at back ipsilateral locations.

Of the three notches, N3 was the most consistent, appearing usually as a spectral dip between P3 and P4, with a mean value of 11.6 kHz. On the other hand, in accord with the literature, N1 and N2 showed the largest variations across locations, with the characteristic rise in frequency with increasing elevation and the concomitant disappearance of N2 at high elevations; these first two notches therefore presented the greatest difficulties for consistent labelling. The tentative labels in Fig. 3 were decided manually, based on our attempt to maintain smooth frequency trajectories across locations.

Sensitivity analysis & pattern grouping

Fig. 4 shows the same set of baseline PRTFs, but with features labelled after analysis of their pinna sensitivity patterns. In particular, by setting the minimum correlation threshold to 0.8 in the grouping algorithm, 209 of the sensitivity patterns were grouped into 14 distinct categories (leaving 25 patterns insufficiently correlated with any other). The threshold value of 0.8 was determined experimentally: more conservative values (higher than 0.8) resulted in only sparsely populated groups and a greater number of insufficiently correlated patterns, while values lower than 0.8 resulted in groups with more diverse and increasingly dissimilar patterns. The value 0.8 was therefore chosen as a compromise yielding a reduction in the total number of distinct sensitivity patterns while retaining meaningful results.

The following sections discuss the patterns that emerged from this grouping, for each acoustic feature in turn. To visualise the results of the sensitivity analysis, in Figs. 5 and 6 the relative frequency shifts for each group mean at a time were projected onto the pinna surface by mapping the range of values to a colour scale, with cool and warm colours representing negative and positive frequency shifts respectively, and with the colour intensity being proportional to the magnitude of the shift. To facilitate comparison of our results with the literature, note that regions of negative and positive sensitivity can be associated with acoustic pressure nodes (near zero pressure) and anti-nodes (maxima), respectively. Note also that these figures show the DB60 pinna and the adjacent patch of KEMAR's head in a 2 mm voxelated representation, i.e., exactly as seen by the FDTD simulation algorithm.

P1

The three mean patterns related to the first PRTF peak P1 are shown at the top of Fig. 5. The main pattern, labelled P1-a, accounts for the majority of P1 peaks (refer to Fig. 4 to identify their locations), at an average frequency of 5.0 kHz. This pattern clearly reveals that a surface perturbation in any part of the concha and cymba cavities, as well as the lower part of the crus of helix, tended to raise P1 frequency; while a perturbation of the pinna surface roughly surrounding those regions tended to lower P1 frequency. This sensitivity pattern is indeed quite similar to the so-called concha depth resonance obtained from pressure distribution patterns (Shaw, 1997; Kahana & Nelson, 2000, 2006; Takemoto *et al*., 2009).

Extending the results reported in the literature, our sensitivity analysis revealed an additional pattern labelled here as P1-b.

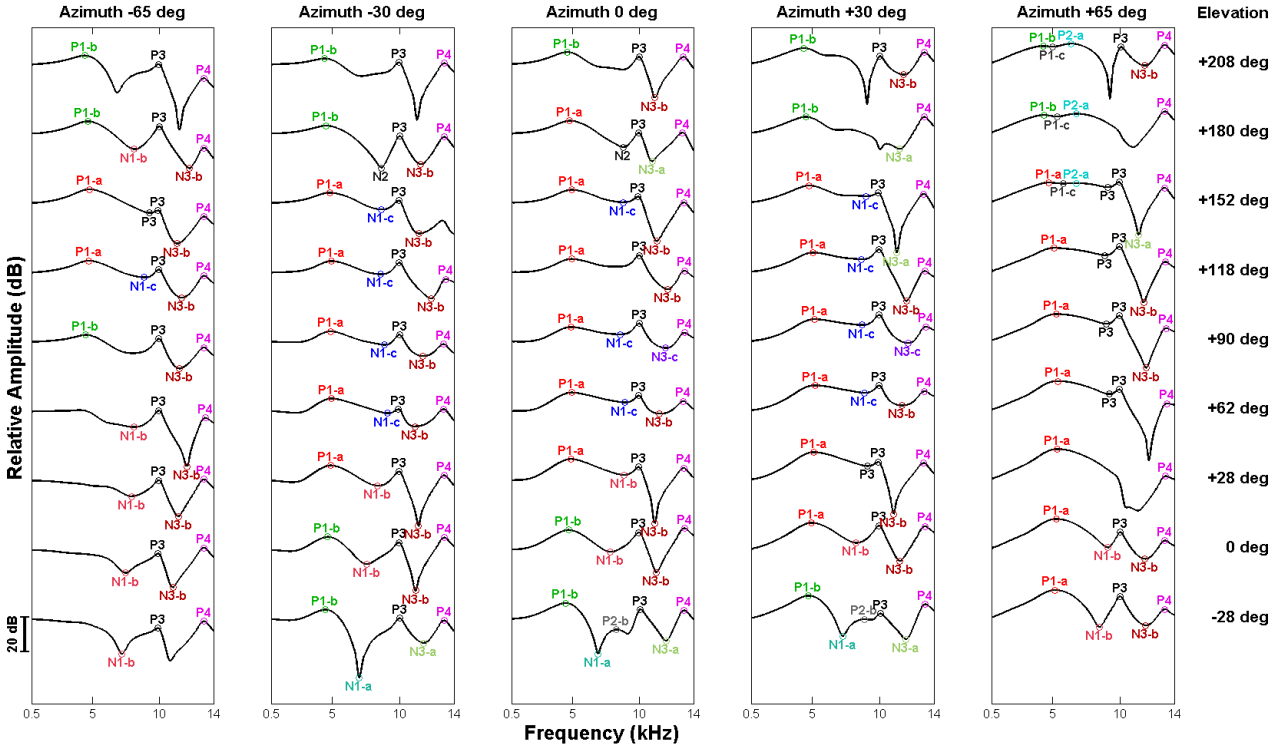

Figure 4. Group labels assigned to the 209 PRTF peaks and notches whose pinna sensitivity patterns were sufficiently similar (as defined by a minimum intra-group linear correlation of 0.8, resulting in 14 distinct groups). For clarity, the 25 peaks and notches whose pinna sensitivity patterns did not sufficiently correlate with any other pattern, are not labelled.

The 15 acoustic features contributing to this pattern were P1 peaks at locations on or below the horizontal plane both in front and behind, and one location at the far contralateral side (cf. Fig. 4). Kahana & Nelson (2000) already showed that the P1 resonance weakens slightly at those locations (at least for grazing incidence). Our P1-b pattern reveals that as the strength of resonance wanes, the regions of positive sensitivity shift away from the concha base toward its anterior rim (including the tragus, the crus of helix, and the concha floor), and the regions of negative sensitivity move outward to the helix. Thus our results suggest a slightly enlarged physical volume of resonance and greater coupling with the free-field, which explain respectively the slightly lower resonance frequency of 4.5 kHz and the broader bandwidth of the P1 peak at those locations.

The third pattern, labelled P1-c, is similar to P1-a but with apparently reversed colours. In Fig. 4 it is shown that all three of the acoustic features contributing to this pattern were in fact small spectral dips lying adjacent to P1. Rather than a true or independent notch, our analysis therefore reveals that the centre-frequency of this spectral dip simply shifted up/down in frequency as P1 shifted down/up. Hence, P1-c is approximately a reversed version of the main P1-a resonance pattern, albeit with a slightly smaller volume brought about by the spectral dip having a higher characteristic frequency of 5.4 kHz.

P2

The two mean patterns related to the second PRTF peak P2 are also shown in Fig. 5. As already mentioned, P2 was problematic in that it appeared in only 7 PRTFs, and not always as a clearly defined peak. Kahana & Nelson (2000) had also noted that the DB60 P2 is excited much less efficiently than the other resonances, although they went on to identify it as the first vertical mode with its strongest response at a source location of +41° grazing incidence. Our sensitivity analysis resulted in five of the observed peaks being categorised into two groups: the P2-a pattern which accounts for the three P2 peaks at ipsilateral back locations, with an average frequency of 6.6 kHz; and the P2-b pattern which accounts for the two P2 peaks at low-front locations with an average frequency of 8.6 kHz (cf. Fig. 4). Despite their differences, what these two patterns have in common is a narrow region of negative sensitivity at or just above the cymba, separating an upper region and a lower region of positive sensitivity. This is in accord with the so-called first mode of vertical resonance obtained from pressure patterns in previous studies. Our results extend previous findings, by showing that for incidence from ipsilateral back locations the concha cavity and the inner-front part of the helix are involved in creating the vertical resonance (P2-a); while for incidence from low-front locations the involvement of the concha is weakened and the upper anti-node of the vertical resonance lies in the triangular fossa (P2-b).

P3 & P4

The mean patterns related to the third and fourth PRTF peaks P3 and P4 are also shown in Fig. 5. As mentioned earlier, these two peaks were the most stable of the acoustic features. Indeed, our grouping algorithm identified 48 patterns as belonging to the P3 group, with an average centre-frequency of 9.8 kHz; and 44 patterns as belonging to the P4 group, with an average centre-frequency of 13.3 kHz. It is interesting to note that six of the acoustic features grouped together with P3 were in fact spectral dips adjacent to P3 and originally labelled as either N1 or N2. Our sensitivity analysis therefore suggests that those dips are not independent notches, but rather spectral valleys that simply follow the frequency shifts of their neighbouring P3 peak.

More importantly, the P3 and P4 patterns in Fig. 5 show resonance characteristics similar to those reported in the lit-

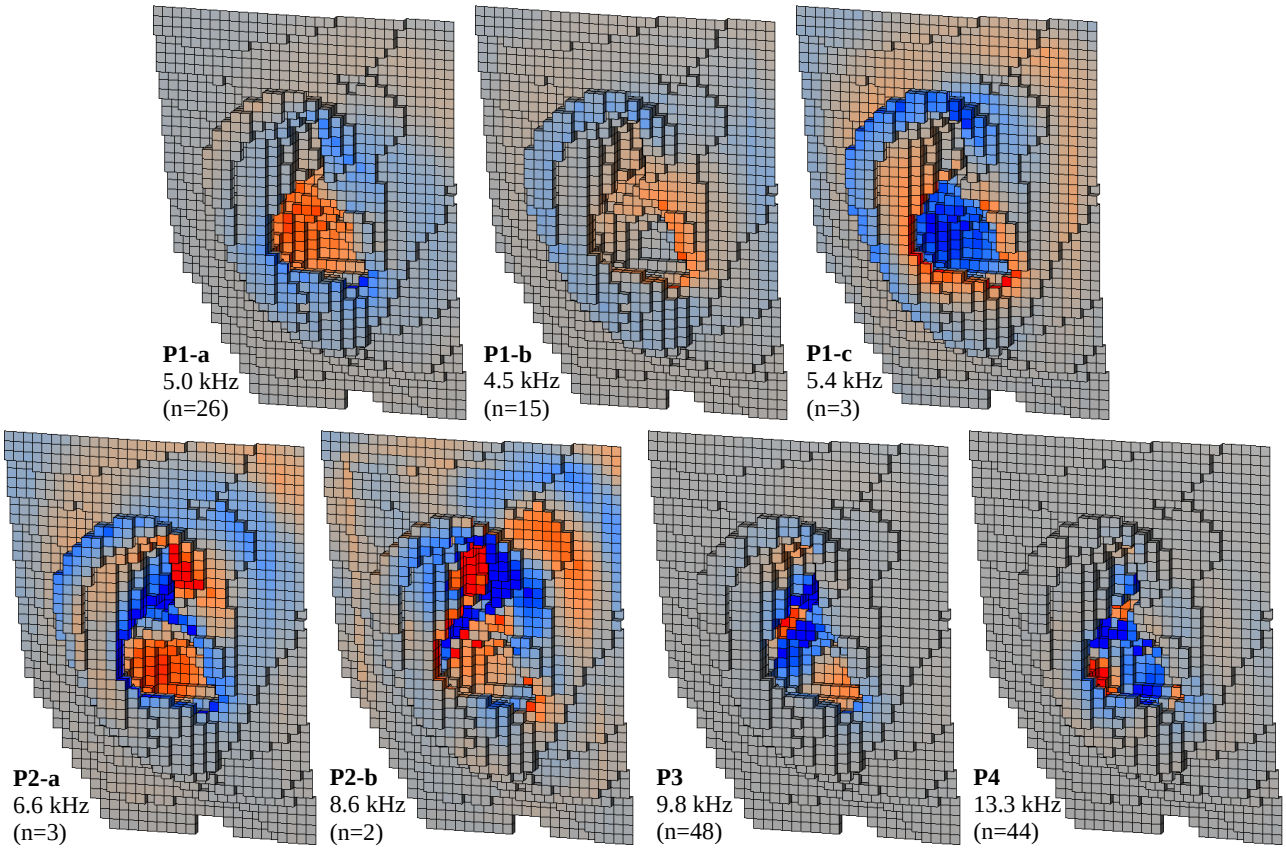

Figure 5. Mean pinna sensitivity patterns for the seven groups of acoustic features related to PRTF resonances P1, P2, P3 and P4. Indicated beside each panel is the corresponding group label (cf. Fig. 4), the average centre-frequency of the corresponding acoustic features, and the number of features whose sensitivity patterns contributed to the mean. For consistency, the colour scale is identical across all patterns, with cold/grey/warm colours indicating negative/zero/positive frequency shifts respectively, and with maximum colour saturation at 0.29% relative frequency shift (twice the average standard-deviation of all distributions).

erature cited earlier. In particular, P3 appears as the second vertical resonance mode, with two regions of negative sensitivity (pressure nodes) dividing three regions of positive sensitivity (pressure anti-nodes) at the lower part of the concha, the cymba, and above the triangular fossa. P4 appears as the first two-dimensional (horizontal and vertical) mode, with a vertical band of negative sensitivity (pressure node) dividing the concha horizontally into a front region and a back region of positive sensitivity (pressure anti-nodes), and a further two regions of negative sensitivity dividing the concha from the upper part of the cymba and the region above the triangular fossa.

N1

The top panels in Fig. 6 show the three mean patterns related to the notch N1. As shown in Fig. 4, pattern N1-a occurred for incidence from the three low-front locations, with a mean centre-frequency of 7.1 kHz; pattern N1-b occurred for 12 locations mainly in the front hemisphere on or close to the horizontal plane, with a mean centre-frequency of 8.1 kHz; and pattern N1-c occurred for 12 locations mainly at high elevations, with a mean centre-frequency of 8.8 kHz (note that this group includes four notches that we had unknowingly labelled as N2). Thus, our analysis resulted in a subdivision of the N1 sensitivity patterns into three groups differentiated mainly by elevation angle.

In Fig. 6, pattern N1-a appears to have two main regions of positive sensitivity: one large region covering the cymba and triangular fossa, and a smaller region around the tragus and intertragic notch. In agreement with Takemoto *et al*.'s (2009) "counter-cancelling" mechanism of N1 generation, assuming sound waves incident from low-front locations to be reflected back from the cymba-fossa region to cancel the direct waves near the ear-canal entrance, any outward perturbation of that region's surface should result in a shorter delay time and an upward shift in notch frequency, as observed. Also in agreement with Lopez-Poveda & Meddis (1996), the incident waves are not only direct and reflected, but also diffracted: indeed, from front locations not far from the median plane, the so-called direct wave must reach the ear-canal entrance only after diffracting (or crawling) around the tragus and intertragic notch, so that any additional protuberance of those structures would delay the arrival of the direct wave, thus having a similar effect of shifting the N1 frequency upward, as observed by the positive sensitivity in that region.

Though generally similar, pattern N1-b is perhaps closer to the more traditional view of N1 being caused by reflections from the back wall of the concha (e.g., Raykar *et al*., 2005). Indeed, the pattern shows that for incidence from near-horizontal elevations in the front hemisphere, the region of positive sensitivity lies in the cymba and on the upper back wall of the concha. Additionally, the pattern reveals a weaker region of positive sensitivity around the tragus that is probably associated with the same diffraction phenomenon discussed in relation to the N1-a pattern.

In contrast with the single regions of positive sensitivity in the upper parts of the pinna shown in the N1-a and N1-b patterns, pattern N1-c displays two such regions, separated by a region of strongly negative sensitivity in the triangular fossa. For sound waves incident from above and behind,

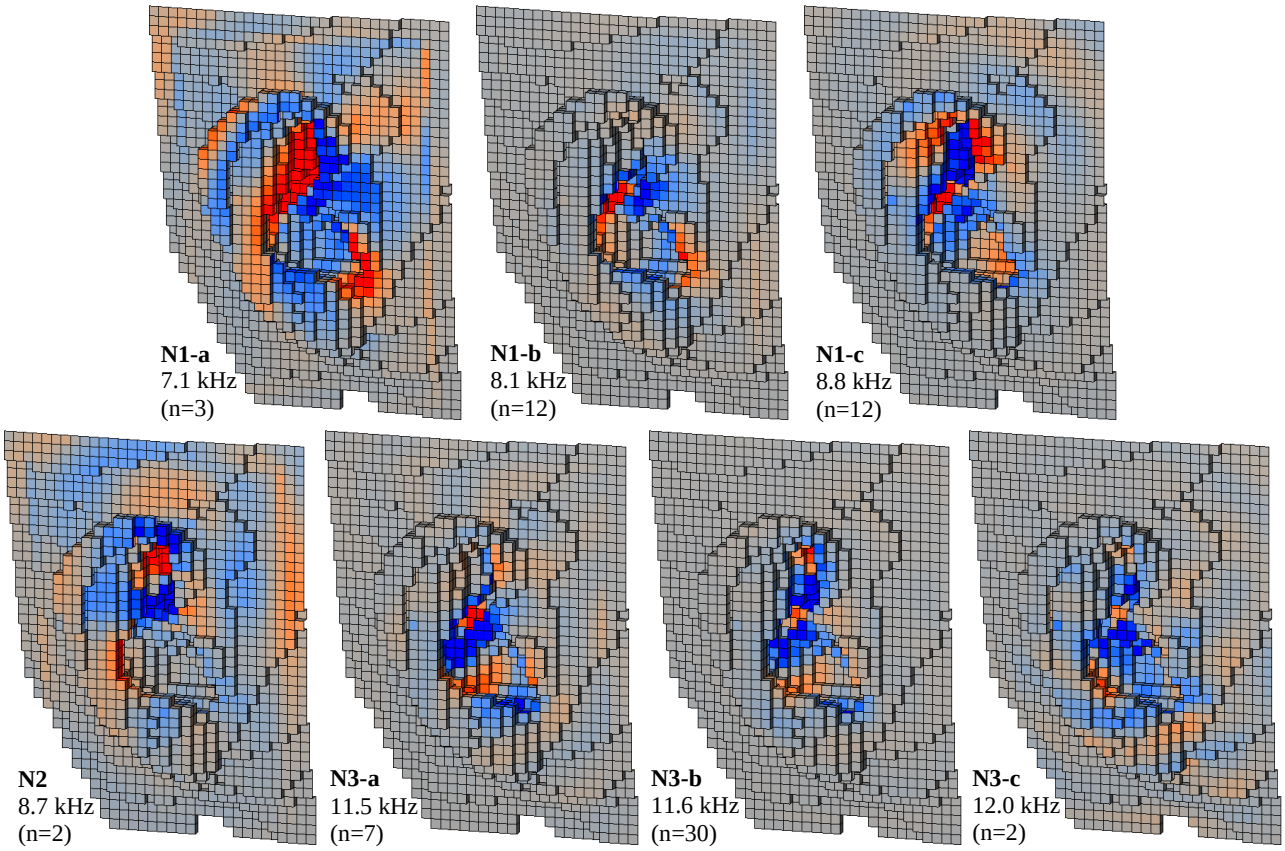

Figure 6. Mean pinna sensitivity patterns for the seven groups of acoustic features related to PRTF anti-resonances N1, N2 and N3. Indicated beside each panel is the corresponding group label (cf. Fig. 4), the average centre-frequency of the corresponding acoustic features, and the number of features whose sensitivity patterns contributed to the mean. For consistency, the colour scale is identical across all patterns, with cold/grey/warm colours indicating negative/zero/positive frequency shifts respectively, and with maximum colour saturation at 0.29% relative frequency shift (twice the average standard-deviation of all distributions).

Takemoto *et al.* (2009) suggested that N1 is generated by an "intercept-cancelling" mechanism whereby resonating structures in the upper pinna cavities absorb incoming waves at the resonance frequency, thus preventing them from arriving at the ear-canal entrance. Pattern N1-c suggests that the resonance of the upper cavities causing a notch around 8.8 kHz at high elevations by this mechanism, involves the lower part of the cymba, and the regions on the inner parts of the helix describing an extended arc above the triangular fossa.

N2

A comparison of Figs. 3 and 4 shows that of the 15 notches initially labelled as N2, six were grouped together with other features (four with N1, two with P3) and seven remained insufficiently correlated with any other feature, leaving only the two N2 notches at back locations. The mean pattern of these latter N2 notches, with an average centre-frequency of 8.7 kHz, is shown in the bottom left panel of Fig. 6.

The main feature of the N2 pattern is a region of strongly positive sensitivity in the upper part of the triangular fossa, closely surrounded by regions of negative sensitivity. This pattern suggests a physically isolated resonance, situated in the small cavity of the upper triangular fossa. However, it is presently unclear how such a local resonance in that upper pinna cavity could cause either absorption or cancellation of sound waves incident from behind and travelling towards the entrance of the ear-canal.

The N2 pattern additionally reveals a weaker region of positive sensitivity along the antihelix at the back of the concha. This could be explained in terms of the same diffraction phenomenon discussed earlier in relation to the N1-a pattern, where a protuberance of that region would effectively delay the arrival of the incoming wave at the entrance of the ear-canal. However, in the absence of any obvious counter-cancellation mechanism for N2, this explanation remains tentative.

N3

Our grouping algorithm identified three patterns of sensitivity for N3, as shown in the bottom right panels of Fig. 6. The main pattern was N3-b, which was common across a wide range of 30 locations, with an average centre-frequency of 11.6 kHz. Pattern N3-c occurred for only two locations above, with an average centre-frequency of 12.0 kHz; while pattern N3-a occurred for 7 seemingly unrelated locations at either low-front or back-ipsilateral, with a lower average centre-frequency of 11.5 kHz.

Despite their separation into three groups, these N3 patterns have the following features in common: three main regions of negative sensitivity (at the concha floor, the crus of helix, and the lower part of the triangular fossa) interleaved with three main regions of positive sensitivity (at the lower-back of the concha, in the cymba, and in the upper part of the triangular fossa or inner-front of the helix).

These patterns have some similarities with the P4 pattern discussed earlier, although they are lacking a clear horizontal division of the concha as exhibited in the P4 pattern. At present, we can only speculate that the N3 patterns suggest a

higher mode of resonance involving these parts of the pinna, and that the resonance pattern either creates a node near the ear-canal entrance, or otherwise absorbs or cancels incoming waves at the resonance frequency.

CONCLUSIONS

FDTD simulation was used to perform acoustic sensitivity analysis of the centre-frequencies of 234 PRTF peaks and notches up to 14 kHz and across a wide range of spatial locations, in response to micro-perturbations along the entire surface of the DB60 pinna and an adjacent patch of KEMAR's head. A grouping algorithm was then applied to the resulting 234 patterns of pinna sensitivity, reducing the data to 7 mean patterns related to the first four peaks, and 7 mean patterns related to the first three notches. Given that the patterns within each group are by definition sufficiently similar, we may assume that the group mean patterns (in Figs. 5 & 6) are a fair representation of the physical mechanisms involved in generating the related resonances or anti-resonances.

The mean sensitivity patterns for the PRTF peaks confirmed and extended the results of previous measurements and simulations of acoustic pressure distributions, attributing P1 to a depth resonance of the combined concha-cymba cavities; P2 and P3 to the first and second vertical modes of resonance involving the concha, cymba, and upper parts of the pinna; and P4 to a more complex mode of resonance involving both horizontal and vertical components. Our results further extended previous findings, by identifying directional variations of the P1 and P2 resonance patterns.

The mean sensitivity patterns for the PRTF notches also confirmed and extended previous work. The patterns for N1 revealed an elevation dependence of the physical mechanism responsible for generating the anti-resonance. Our results were in agreement with the "counter-cancelling" and "intercept-cancelling" mechanisms proposed by Takemoto *et al*. (2009), and with the importance of diffraction as advocated by Lopez-Poveda & Meddis (1996). The mean patterns for N2 & N3 also revealed the parts of the pinna associated with those anti-resonances, although a complete understanding of their generative mechanisms awaits deeper investigations.

A major contribution of this study was to show that sensitivity analysis with the aid of numerical simulation is a powerful tool for revealing the parts of the pinna that are most strongly affiliated with each of the PRTF acoustic features. We hope that these methods can, in combination with more conventional investigations of acoustic pressure distributions, help to better explain the physical mechanisms of peak and notch generation in the pinna.

We plan to extend this work by using the sensitivity patterns to predict the best *combination* of single-voxel perturbations that would be necessary to effect any particular combination of shifts in acoustic features. We are also planning further research to explore inter-individual variations in pinna sensitivity patterns, with geometry data measured accurately by magnetic resonance imaging (MRI) of human ears. Clarification of the physical causes of individual differences in PRTF or HRTF features should have a profound impact on establishing the most important physiological measurements needed to achieve personalisation of HRTFs for diverse applications in spatial audio.

ACKNOWLEDGEMENTS

We are indebted to Dr. Yuvi Kahana for kindly providing his measurements of the KEMAR head and DB60 pinna; and to Prof. Kazuhiro Iida for invaluable support and discussions.

REFERENCES

1. V.R. Algazi, R.O. Duda, R. Duraiswami, N.A. Gumerov and Z. Tang, "Approximating the head-related transfer function using simple geometric models of the head and torso" *J. Acoust. Soc. Am.* **112**(5), 2053–2064 (2002)
2. J. Blauert, *Spatial hearing* (Revised Edition, MIT Press, Cambridge, 1997)
3. C.P. Brown and R.O. Duda, "A structural model for binaural sound synthesis" *IEEE Trans. on Speech and Audio Process.* **6**(5), 476–488 (1998)
4. M.D. Burkhard and R.M. Sachs, "Anthropometric manikin for acoustic research" *J. Acoust. Soc. Am.* **58**(1), 214–222 (1975)
5. J. Hebrank and D. Wright, "Spectral cues used in the localization of sound sources on the median plane" *J. Acoust. Soc. Am.* **56**(6), 1829–1834 (1974)
6. K. Iida, M. Itoh, A. Itagaki and M. Morimoto, "Median plane localization using a parametric model of the head-related transfer function based on spectral cues" *Applied Acoustics* **68**, 835–850 (2007)
7. Y. Kahana and P.A. Nelson, "Spatial acoustic mode shapes of the human pinna" in *Proc. AES 109th Convention*, Los Angeles, USA, 24 pp. (2000)
8. Y. Kahana and P.A. Nelson, "Numerical modelling of the spatial acoustic response of the human pinna" *J. Sound and Vibration* **292**, 148–178 (2006)
9. E.A. Lopez-Poveda and R. Meddis, "A physical model of sound diffraction and reflections in the human concha" *J. Acoust. Soc. Am.* **100**(5), 3248–3259 (1996)
10. P. Mokhtari, H. Takemoto, R. Nishimura and H. Kato, "Efficient computation of HRTFs at any distance by FDTD simulation with near to far field transformation" in *Proc. Autumn Meet. of the Acoust. Soc. Japan*, Fukuoka, Japan, Paper 1-8-12, 611-614 (2008)
11. P. Mokhtari, H. Takemoto, R. Nishimura and H. Kato, "Acoustic simulation of KEMAR's HRTFs: verification with measurements and the effects of modifying head shape and pinna concavity" in *e-Proc. Int. Workshop on the Principles and Applications of Spatial Hearing* (eISBN 978-981-4299-31-2), 4 pp. (2009)
12. P. Mokhtari, H. Takemoto, R. Nishimura and H. Kato, "Optimum loss factor for a perfectly matched layer in finite difference time domain acoustic simulation" *IEEE Trans. on Audio, Speech and Lang. Process.* (in print, 2010)
13. V.C. Raykar, R. Duraiswami and B. Yegnanarayana, "Extracting the frequencies of the pinna spectral notches in measured head related impulse responses" *J. Acoust. Soc. Am.* **118**(1), 364–374 (2005)
14. M.R. Schroeder, "Determination of the geometry of the human vocal tract by acoustic measurements" *J. Acoust. Soc. Am.* **41**(4), 1002–1010 (1967)
15. E.A.G. Shaw and R. Teranishi, "Sound pressure generated in an external-ear replica and real human ears by a nearby point source" *J. Acoust. Soc. Am.* **44**(1), 240–249 (1968)
16. E.A.G. Shaw, "Acoustical characteristics of the outer ear" in *Encyclopedia of Acoustics* ed. M.J. Crocker, (Wiley, New York, 1997) pp. 1325–1335
17. A. Taflove and M.E. Brodwin, "Numerical solution of steady-state electromagnetic scattering problems using the time-dependent Maxwell's equations" *IEEE Trans. on Microwave Theory & Techniques* **23**(8), 623–630 (1975)
18. H. Takemoto, P. Mokhtari, H. Kato, R. Nishimura and K. Iida, "Pressure distribution patterns on the pinna at spectral peak and notch frequencies of head-related transfer functions in the median plane" in *e-Proc. Int. Workshop on the Principles and Applications of Spatial Hearing* (eISBN 978-981-4299-31-2), 4 pp. (2009)